Solar Nanocomposites with Complementary Charge Extraction Pathways for Electrons and Holes: Si Embedded in ZnS

Stefan Wippermann,[1,2,3] Márton Vörös,[2,3] Adam Gali,[4,5] Francois Gygi,[6] Gergely T. Zimanyi,[3] and Giulia Galli[7]
[1]*Interface Chemistry and Surface Engineering Department, Max-Planck-Institute for Iron Research GmbH, Max-Planck-Straße 1, 40237 Düsseldorf, Germany*
[2]*Chemistry Department, University of California, Davis, California 95616, USA*
[3]*Physics Department, University of California, Davis, California 95616, USA*
[4]*Department of Atomic Physics, Budapest University of Technology and Economics, Budafoki út 8., H-1111 Budapest, Hungary*
[5]*Institute for Solid State Physics and Optics, Wigner Research Centre for Physics, Hungarian Academy of Sciences, P.O. Box 49, H-1525 Budapest, Hungary*
[6]*Department of Computer Science, University of California, Davis, California 95616, USA*
[7]*Institute for Molecular Engineering, University of Chicago, Illinois 60637, USA*
(Received 9 October 2013; published 11 March 2014)

We propose that embedding silicon nanoparticles (NP) into amorphous, nonstoichiometric ZnS leads to promising nanocomposites for solar energy conversion. Using *ab initio* molecular dynamics simulations we show that, upon high temperature amorphization of the host chalcogenide, sulfur atoms are drawn to the NP surface. We find that the sulfur content may be engineered to form a type II heterojunction, with complementary charge transport channels for electrons and holes, and that sulfur capping is beneficial to lower the nanoparticle gap, with respect to that of NPs embedded in oxide matrices. Our analysis is conducted using density functional theory with local and hybrid functionals and many body perturbation theory at the *GW* level.

DOI: 10.1103/PhysRevLett.112.106801 PACS numbers: 73.22.-f, 71.35.-y, 73.63.Bd, 78.67.Bf

One of the paradigms of making nanoparticle-(NP-) based solar energy conversion devices is to embed the NPs in solid matrices to increase the efficiency of charge extraction and transport [1]. The host matrix can be either crystalline or amorphous. However, a detailed understanding of the influence of the embedding matrix on the absorption of sunlight by the nanoparticle and the role of the nanoparticle-matrix interface remain elusive at present. A primary concern is the recombination of the photoinduced electrons and holes. In crystalline solar cells even ppm concentrations of certain defects and impurities cause substantial recombination, leading to severe losses of the energy-conversion efficiency [2]. In NP-based solar cells defects may be present at the NP-matrix interfaces and possibly induce excessive recombination, especially given the large total interfacial area.

One of the design principles to reduce charge recombination is to spatially separate the photoinduced electrons and holes. This may be achieved, e.g., by creating a type II heterojunction between the NP and the matrix, where the conduction and valence states are localized in different regions of the nanocomposite, either on the guest NP or on the host matrix.

Epitaxial quantum dots can be designed to support such type II band offsets [3], and core-shell NP systems with type II band alignments have been identified [4,5]. In addition, quantum-dot sensitized solar cells with type-II interfaces have been reported in the literature [6–8]. However, in the context of a NP and its embedding matrix, clear strategies to design band offsets are not yet available. Moreover, many known matrix-embedded NP systems form type I heterojunctions with the gap of the NP falling inside that of the host material. For example, Si NPs embedded in SiO_2 form a type I interface [9–11]. Recently, we showed that type II interfaces may be realized by strain engineering when Si-NPs are embedded in amorphous SiO_2 [12]. However, that study was not considering transport channel optimization.

In this Letter, we report *ab initio* calculations of the electronic properties of Si nanoparticles embedded in amorphous ZnS, using density functional (DFT) and many body perturbation theory (MBPT). We show that it is possible to design nonstoichiometric nanocomposites that exhibit a type II heterojunction at ambient conditions, unlike bulk crystalline Si and ZnS, with complementary charge transport channels, for electrons and holes. In addition, in such nanocomposites the electronic gap of the Si nanoparticles is reduced compared to that of hydrogenated Si NPs and Si dots embedded in SiO_2 [12]. We hence propose that Si NPs embedded in II-VI chalcogenides are promising candidates for light absorbers in solar energy conversion devices.

We carried out density functional theory (DFT) calculations within the local density (LDA) [13] and PBE0 [14] approximations, using plane wave basis sets and norm-conserving pseudopotentials [15] with an energy cutoff of 80 Ry. Geometrical optimizations and molecular dynamics (MD) simulations were performed at the LDA level, and

hybrid functionals and MBPT calculations were carried out using LDA optimized geometries. *Ab initio* MD and PBE0 calculations were done with the QBOX code [16]. QUANTUM ESPRESSO [17] was used for electronic structure analyses. Quasiparticle energies within the *GW* scheme [18] were obtained employing the approach of Nguyen *et al.*, which avoids the explicit calculation of empty electronic states and the inversion of large dielectric matrices [19,20].

In order to obtain realistic models of Si NPs embedded in *a*-ZnS matrices, we first built a periodically repeated cubic cell of crystalline ZnS in the zinc blende structure, at the LDA equilibrium lattice constant of Si (5.39 Å). We then replaced all Zn and S atoms within a given spherical region by Si atoms. The center and radius of the sphere were chosen to obtain Si NPs with each surface atom having at most two Si-Zn or Si-S bonds; this resulted in 1.1, 1.3, 1.6, and 1.9 nm NPs, denoted as Si_{35}, Si_{66}, Si_{123} and Si_{172}, respectively. The Si_{35} and $Si_{66–172}$ NPs were embedded in unit cells corresponding to 216 and 512 atoms, respectively. Next, the size of the simulation volume was adjusted while keeping the radius of the Si NP fixed, so as to obtain Si and ZnS bond lengths equal to their respective equilibrium bulk values of 5.39 and 5.34 Å. The bond lengths within the interfacial region were initially set at 5.365 Å, according to Vegard's law. Finally, an additional adjustment of the simulation volume was performed to accommodate the thermal expansion of Si and ZnS at high temperature, yielding a volume increase of ~3.4%. The resulting configurations were used to start annealing cycles to amorphize the ZnS matrix, employing *ab initio* MD. First, the temperature T of the ZnS matrix was raised [21] to 2400 K, while keeping the positions of the Si atoms fixed at their initial coordinates to preserve the integrity of the NP. This temperature is significantly higher than the melting point of ZnS (1650 °C to 1900 °C [22,23]), and it is required to melt ZnS in our small simulation cells, in the absence of point defects. Upon melting we observed diffusion of Zn and S atoms. Subsequently, T was lowered, and below 600 K, the Si atoms were allowed to move as the system was cooled further. The entire annealing processes span 22 and 10 ps for the Si_{35} and $Si_{66–172}$ NPs, respectively.

During the annealing cycles, S atoms were drawn to the Si NP from the matrix, leading to the formation of a sulfur shell on the nanoparticle surface. We found that the S atoms within this sulfur shell were threefold coordinated, as opposed to their fourfold coordination within the matrix. They formed one S-Si and two S-Zn bonds, leaving two electrons to form a lone pair state. Such a state is shown in Fig. 1 for the case of Si_{35} embedded in $Si_{35}Zn_{81}S_{100}$.

As S atoms migrated to the Si surface, Zn clusters formed within the matrix, accompanied by the appearance of electronic states in the nanocomposite gap; such states undermine the utility of the system for solar applications that require the existence of a well defined electronic gap.

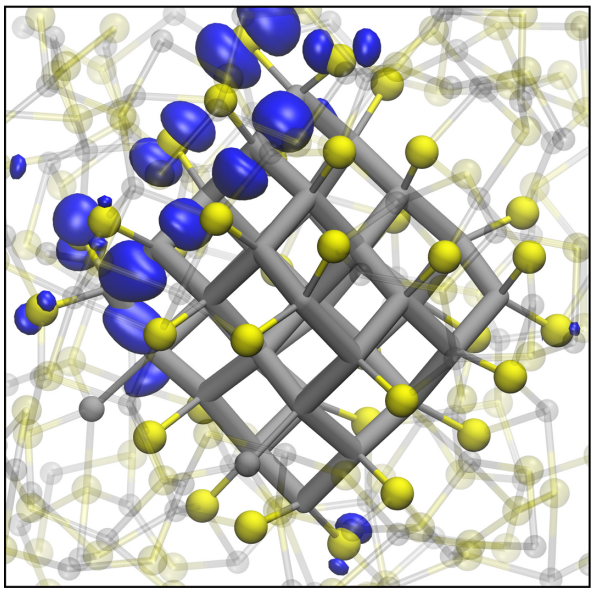

FIG. 1 (color online). Ball and stick representation of a Si nanoparticle (Si_{35}, gray rods) embedded in an *a*-ZnS matrix ($Zn_{81}S_{100}$), showing the sulfur atoms (yellow spheres) capping its surface. The highest occupied orbital (whose square modulus is shown in blue) is localized on the surface layer and composed of S lone pairs.

To overcome this problem, we generated nonstoichiometric $Zn_{1-x}S_{1+x}$ nanocomposites by replacing some of the Zn atoms of the metallic Zn clusters with S atoms and performing additional annealing cycles. The procedure was repeated until most Zn clusters were removed. The resulting nanocomposites are $Si_{35}Zn_{81}S_{100}$ and $Si_{123}Zn_{188}S_{201}$, and they are comprised of three regions: Si NPs, sulfur shells around the NPs, and an essentially stoichiometric amorphous ZnS matrix free of Zn clusters.

Figure 2(a) shows the electronic densities of states (EDOS) of both stoichiometric (dotted lines) and non-stoichiometric Si-NP/*a*-ZnS composite structures as a function of the NP size, computed at the LDA level of theory. The corresponding gaps of the Si NP are shown in Fig. 2(b), where they are compared with those of Si dots embedded in *a*-SiO_2 (Ref. [12]). We observe that the gap of the Si-NP/*a*-ZnS nanocomposite is much reduced relative to the 1.9 eV gap of bulk *a*-ZnS (also obtained within the LDA). The gaps quoted here are effective quantities, defined with an EDOS $D(\epsilon)$ threshold,

$$\int_{\mathrm{VBM}}^{E_F} D(\epsilon)d\epsilon = \int_{E_F}^{\mathrm{CBM}} D(\epsilon)d\epsilon = \Delta \int_{-\infty}^{E_F} D(\epsilon)d\epsilon, \quad (1)$$

where E_F is the Fermi energy of the composite system, located inside the gap, and Δ is a suitably chosen threshold parameter to discard midgap states.

The reduction of the gap is crucial for utilizing the Si nanoparticles for solar energy conversion. While bulk Si

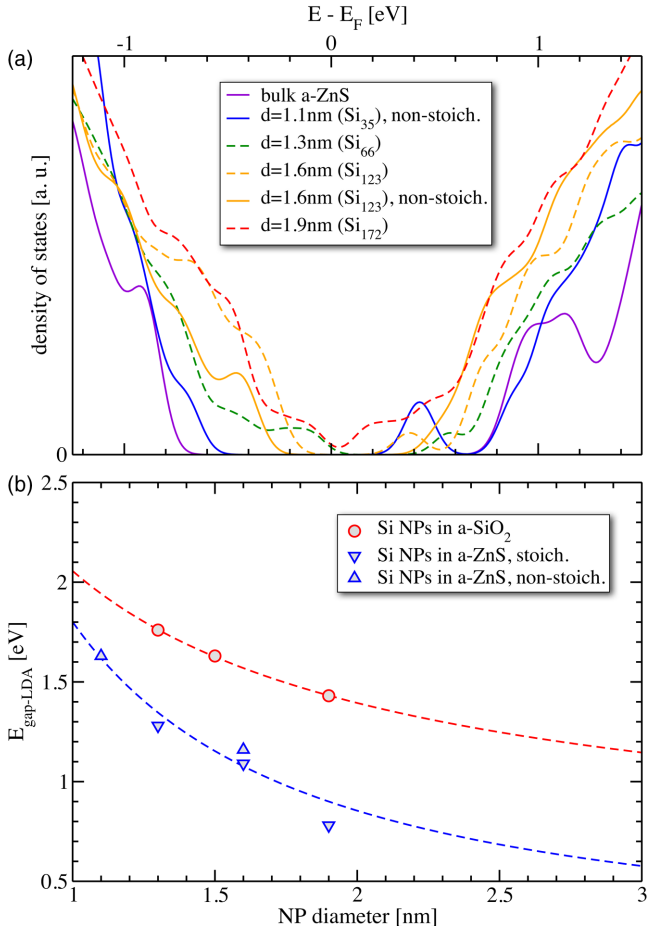

FIG. 2 (color online). (a) Densities of states (EDOS) renormalized by the number of electrons in the respective model and (b) electronic gaps of Si NPs embedded into a-ZnS as a function of the NP diameter, computed using LDA, as defined by Eq. (1). The electronic gaps of Si NPs embedded in a-SiO_2 (from Ref. [12]) are shown for comparison.

has a 1.1 eV gap that is near optimal for solar applications, quantum confinement increases the gap to higher values as the diameter is reduced, with values above 2–2.5 eV for small NPs (< 3 nm in diameter), making them unable to absorb the majority of the solar spectrum [24,25].

We now turn to the discussion of the character of the states at the valence band maximum (VBM) and conduction band minimum (CBM) of the nanocomposite. Figure 3(a) shows the total EDOS of a sample with a Si_{123} NP embedded into a-ZnS. We selected the 1.6 nm Si_{123} NP as it is the largest one that fits in our simulations cell, which still has a reasonably large distance between periodic replica (9 Å from NP surface to NP surface). We divided the EDOS into contributions from the NP, sulfur-shell and matrix spatial regions. We defined two spheres: one enclosing the Si NP without its capping sulfur atoms (8 Å) and a second one including the sulfur atoms as well (10 Å). We then considered three regions: (i) the interior of the smallest sphere, (ii) a shell with a thickness of 2 Å between the smallest and the largest spheres, and (iii) the remaining part of the simulation cell. Each electronic state ψ_j was projected onto atomic orbitals ϕ_i centered at atomic positions in the above three regions. The contribution of each electronic state to the EDOS of each region (Ω) $D_\Omega(\epsilon)$, was determined as the sum of the projections of the state (ψ) onto the atomic orbitals (ϕ) in that region, in a narrow energy interval around ϵ,

$$D_\Omega(\epsilon) = \sum_j \sum_{i\in\Omega} |\langle \phi_i | \psi_j \rangle|^2 \delta(\epsilon_j - \epsilon). \qquad (2)$$

The projected densities of states are shown in Fig. 3(a), where energy intervals of 0.1 eV were used. The Figure clearly shows that the states at the bottom of the conduction band (CB) are predominantly localized inside the nanoparticle. The first conduction states that reach into the matrix are located well above the conduction band minimum (CBM). Furthermore, the states at the top of the valence band (VB) are predominantly localized outside the nanoparticle.

Further evidence of the respective localization of valence and conduction band edges is shown in Figs. 3(b) and 3(c), where we report isodensity plots of the square moduli of valence and conduction states, integrated over a 0.5 eV energy interval. These figures show that the electronic conduction states at the CBM are localized inside the NP. Further, the hole states at the VBM are extended over both the S shell and the matrix. This translates into a desired spatial separation between the photoinduced electrons and holes, and indicates that electron and hole transport channels are complementary, thus drastically reducing the probability of recombination.

To verify the robustness of our results, we repeated some of our electronic structure calculations for two samples, $Si_{35}Zn_{81}S_{100}$ and $Si_{123}Zn_{188}S_{201}$, using the PBE0 functional and the bisection technique proposed in Ref. [26]; in the $Si_{35}Zn_{81}S_{100}$ case we also carried out calculations using the GW appoximation. We obtained a larger gap of 3.3 and 2.7 eV (PBE0) vs 1.7 and 1.2 eV (LDA) for the $Si_{35}Zn_{81}S_{100}$ and $Si_{123}Zn_{188}S_{201}$ samples, respectively; we also obtained an essentially rigid shift of the EDOS of the nanocomposites, both for the valence and the conduction bands. In addition, we found that also at the PBE0 level of theory, the state at the CBM is localized on the nanoparticle and that the VBM is in the host matrix.

While in our LDA and PBE0 calculations we included the d electrons in the valence, in our GW calculations we froze them in the core, to reduce the computational effort. Hence we only use our GW results to discuss qualitative trends rather than absolute values of eigenvalues and gaps [27] . Consistent with our PBE0 results, at the GW level we found a rigid shift of both the valence and conduction band EDOS, confirming that the results obtained within LDA are qualitatively robust.

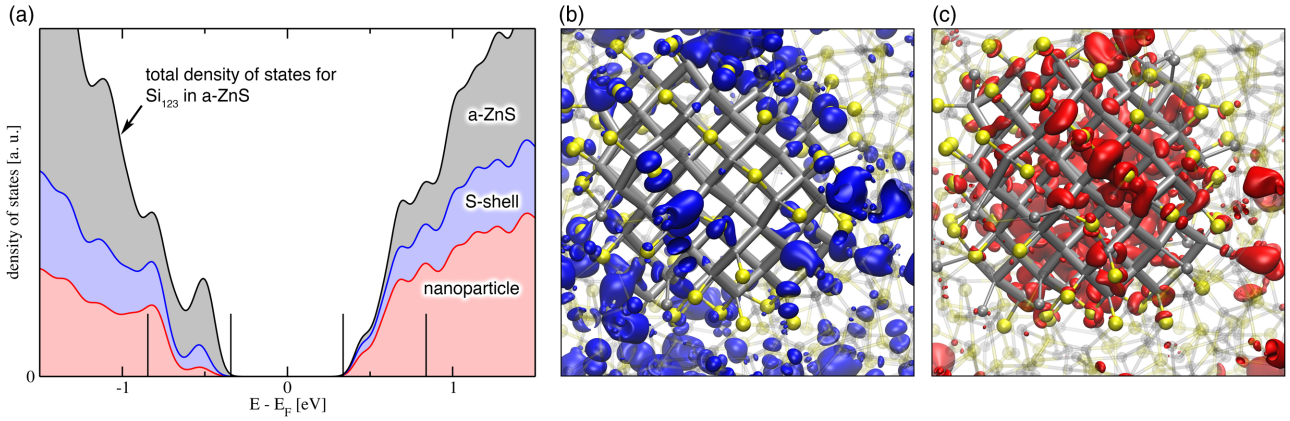

FIG. 3 (color online). (a) Electronic density of states of the Si nanoparticle and host a-ZnS matrix for a sample of $Si_{123}Zn_{188}S_{201}$, partitioned into contributions from the nanoparticle, the surface shell (S shell) and the host matrix (a-ZnS). Isodensity plots of the sum of square moduli of the states at the top of the valence band (blue) and bottom of the conduction band (red) are shown in (b) and (c), respectively. The sums were performed over an energy interval of 0.5 eV, as indicated by vertical bars in (a).

Having established the character of the band edges in the nanocomposite, we computed band offsets using the methodology described, e.g., in Refs. [28,29], and we obtained the spatial dependence of the VBM and CBM energy values as a function of the radial distance from the NP center. We defined the radial local density of states as

$$D(\epsilon, r) = 2\sum_n \overline{|\psi_n(\mathbf{r})|^2}(r)\delta(\epsilon - \epsilon_n), \tag{3}$$

where $\overline{|\psi_n(\mathbf{r})|^2}(r)$ denotes the density of the nth single particle wave function averaged on a surface of a sphere (centered at the nanoparticle center) with radius r. This allows for the determination of the band edge energy values as a function of r,

$$\int_{\mathrm{VBM}(r)}^{E_F} D(\epsilon, r)d\epsilon = \int_{E_F}^{\mathrm{CBM}(r)} D(\epsilon, r)d\epsilon = \Delta \int_{-\infty}^{E_F} D(\epsilon, r)d\epsilon. \tag{4}$$

Figure 4 shows the energy values of the VBM and CBM of the Si_{123} NP embedded in the a-ZnS, as a function of the radial distance from the NP center. The CBM outside the NP is clearly higher than its value inside the NP, by about 0.3 eV. Moreover, the VBM outside the NP is higher than inside by about 0.15 eV. The same type II offsets were obtained with GW calculations [30]. We note that the transition between the bands is sharp and well defined for the conduction band, whereas it is more gradual for the valence band. This gradual increase can be attributed to the electronic states of the sulfur shell. The states induced by the sulfur shell are almost energetically degenerate with the VBM states of the ZnS matrix. Thus the occupied states of the Si NP are located slightly below the ZnS valence band edge. We verified this interpretation in a graphical manner, plotting the square moduli of the individual wave functions (not shown). The results of Fig. 4 confirm those of Fig. 3, showing a type II interface is formed between the Si NPs and the a-ZnS matrix.

In summary, using a combination of first-principles methods, we proposed a strategy to design promising nanocomposites for solar energy conversion, by embedding Si NPs in nonstoichiometric chalcogenide matrices. We found that (i) the embedding of Si NPs into an a-ZnS matrix lowers their quantum-confinement-enhanced gap towards values desirable for solar energy conversion, (ii) using nonstoichiometric host matrices it is possible to design type II matrix-particle heterojunctions, and

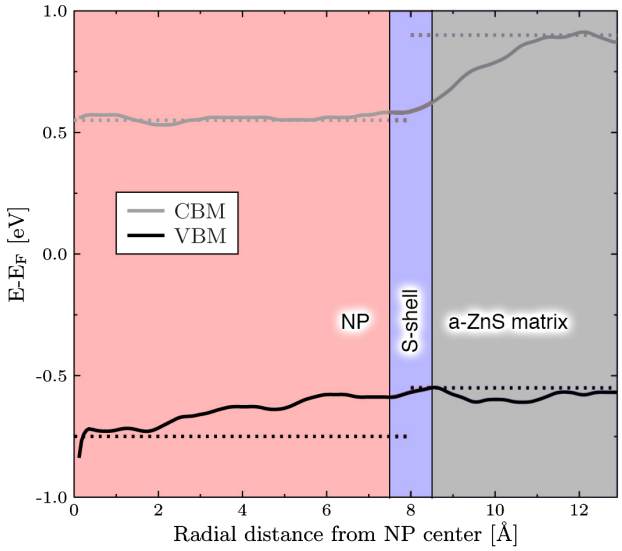

FIG. 4 (color online). Band offsets between the valence band maximum (VBM) and conduction band minimum (CBM) of the Si nanoparticle and host a-ZnS matrix for a sample of $Si_{123}Zn_{188}S_{201}$. The NP/ZnS interface is located at 8 Å, while the cell boundary is located at about 10.8 Å.

(iii) the band edges of these heterojunctions are localized in different portions of the nanocomposite—the CBM is on the NP, while the VBM is in the host matrix, providing the desired spatial separation between electron and hole states and possibly facilitating their extraction. Tantalizingly, a recent experiment has shown that it is indeed possible to enhance the charge mobility, and thereby the charge extraction, of NP composites by infilling the internanoparticle space with an appropriate matrix [31]. However, this experiment considered PbSe NPs and only the electron mobility was shown to become bandlike. To the best of our knowledge ours is the first proposed NP composite where the hole transport channel may show the bandlike characteristics. Work is in progress to investigate mobilities and study in detail transport processes.

The authors wish to thank T. A. Pham for helpful discussions. This research was supported by the NSF-Solar Collaborative (No. DMR-1035468), DOE/BES (Contract No. DE-FG02-06ER46262), and the Deutsche Forschungsgemeinschaft (Grant No. WI3879/1), as well as by supercomputer time provided by NERSC (No. NISE-35687). G. G. acknowledges DOE/BES Grant No. DE-SC0008938. A. G. acknowledges the support from the MTA Lendület Program (Hungarian Academy of Sciences). S. W. acknowledges BMBF Grant No. 13N12972.

[1] A. J. Nozik, Physica (Amsterdam) **14E**, 115 (2002).
[2] M. Green, *Third Generation Photovoltaics: Advanced Solar Energy Conversion*, Springer Series in Photonics (Springer, New York, 2006).
[3] R. B. Laghumavarapu, A. Moscho, A. Khoshakhlagh, M. El-Emawy, L. F. Lester, and D. L. Huffaker, Appl. Phys. Lett. **90**, 173125 (2007).
[4] S. Kim, B. Fisher, H.-J. Eisler, and M. Bawendi, J. Am. Chem. Soc. **125**, 11466 (2003).
[5] J.-S. Lee, M. V. Kovalenko, J. Huang, D. S. Chung, and D. V. Talapin, Nat. Nanotechnol. **6**, 348 (2011).
[6] K. S. Leschkies, R. Divakar, J. Basu, E. Enache-Pommer, J. E. Boercker, C. B. Carter, U. R. Kortshagen, D. J. Norris, and E. S. Aydil, Nano Lett. **7**, 1793 (2007).
[7] J. H. Bang and P. V. Kamat, ACS Nano **3**, 1467 (2009).
[8] P. V. Kamat, J. Phys. Chem. C **112**, 18737 (2008).
[9] K. Seino, F. Bechstedt, and P. Kroll, Phys. Rev. B **82**, 085320 (2010).
[10] G. Seguini, S. Schamm-Chardon, P. Pellegrino, and M. Perego, Appl. Phys. Lett. **99**, 082107 (2011).
[11] G. Seguini, C. Castro, S. Schamm-Chardon, G. BenAssayag, P. Pellegrino, and M. Perego, Appl. Phys. Lett. **103**, 023103 (2013).
[12] T. Li, F. Gygi, and G. Galli, Phys. Rev. Lett. **107**, 206805 (2011).
[13] J. P. Perdew and A. Zunger, Phys. Rev. B **23**, 5048 (1981).
[14] C. Adamo and V. Barone, J. Chem. Phys. **110**, 6158 (1999).
[15] D. R. Hamann, M. Schlüter, and C. Chiang, Phys. Rev. Lett. **43**, 1494 (1979).
[16] F. Gygi, IBM J. Res. Dev. **52**, 137 (2008).
[17] P. Giannozzi, S. Baroni, N. Bonini, M. Calandra, R. Car, C. Cavazzoni, D. Ceresoli, G. L. Chiarotti, M. Cococcioni, I. Dabo, A. D. Corso, S. de Gironcoli, S. Fabris, G. Fratesi, R. Gebauer, U. Gerstmann, C. Gougoussis, A. Kokalj, M. Lazzeri, L. Martin-Samos, N. Marzari, F. Mauri, R. Mazzarello, S. Paolini, A. Pasquarello, L. Paulatto, C. Sbraccia, S. Scandolo, G. Sclauzero, A. P. Seitsonen, A. Smogunov, P. Umari, and R. M. Wentzcovitch, J. Phys. Condens. Matter **21**, 395502 (2009).
[18] L. Hedin, Phys. Rev. **139**, A796 (1965).
[19] H.-V. Nguyen, T. A. Pham, D. Rocca, and G. Galli, Phys. Rev. B **85**, 081101 (2012).
[20] T. A. Pham, H.-V. Nguyen, D. Rocca, and G. Galli, Phys. Rev. B **87**, 155148 (2013).
[21] G. Bussi, D. Donadio, and M. Parrinello, J. Chem. Phys. **126**, 014101 (2007).
[22] A. Addamiano and P. A. Dell, J. Phys. Chem. **61**, 1020 (1957).
[23] R. C. Sharma and Y. A. Chang, J. Cryst. Growth **88**, 193 (1988).
[24] T. van Buuren, L. N. Dinh, L. L. Chase, W. J. Siekhaus, and L. J. Terminello, Phys. Rev. Lett. **80**, 3803 (1998).
[25] G. Ledoux, J. Gong, F. Huisken, O. Guillois, and C. Reynaud, Appl. Phys. Lett. **80**, 4834 (2002).
[26] F. Gygi and I. Duchemin, J. Chem. Theory Comput. **9**, 582 (2013).
[27] See Supplemental Material at http://link.aps.org/supplemental/10.1103/PhysRevLett.112.106801 for additional details on the effect of placing the *d* electrons in the core and on *GW* calculations.
[28] T. Yamasaki, C. Kaneta, T. Uchiyama, T. Uda, and K. Terakura, Phys. Rev. B **63**, 115314 (2001).
[29] T. A. Pham, T. Li, H.-V. Nguyen, S. Shankar, F. Gygi, and G. Galli, Appl. Phys. Lett. **102**, 241603 (2013).
[30] See Supplemental Material at http://link.aps.org/supplemental/10.1103/PhysRevLett.112.106801 for additional details on *GW* calculations.
[31] Y. Liu, J. Tolentino, M. Gibbs, R. Ihly, C. L. Perkins, Y. Liu, N. Crawford, J. C. Hemminger, and M. Law, Nano Lett. **13**, 1578 (2013).